Received: Added at production | Revised: Added at production | Accepted: Added at production

DOI: xxx/xxxx

ARTICLE TYPE

A stable time-dependent mesh method to analyze the linear advection-diffusion equation

Zhang Zhengce[1] | Saad Sultan*[2] | M. Usman[2]

[1]School of Mathematics and Statistics, Xi'an Jiaotong University, Xi'an, Shaaxi, People's Republic of China

[2]School of Mathematics and Statistics, Xi'an Jiaotong University, Xi'an, Shaaxi, People's Republic of China

Correspondence
*Saad Sultan, School of Mathematics and Statistics, Xi'an Jiaotong University, Xi'an 710049, People's Republic of China. Email: saadciit@outlook.com

Present Address
School of Mathematics and Statistics, Xi'an Jiaotong University, Xi'an 710049, People's Republic of China

Abstract

This paper develops the stable adaptive time-dependent mesh scheme for a one-dimensional linear advection-diffusion equation with homogeneous Dirichlet boundary conditions and a sinusoidal initial condition. The aim is to present accurate stable moving nodes finite difference scheme with its stability and convergence. The boundary layer of the flow is exponential therefore difference scheme needs mesh refinement. The moving mesh method analyzes the problem physics and adjusts the mesh according to the problem as it moves nodes in the region of edges. We develop numerical results using four MMPDEs with varying numbers of nodes. A conservative semi-discretization finite difference scheme is used for the spatial derivative and backward Euler difference scheme is employed for the temporal derivative. We have presented five cases in detail to understand the physics of the problem. The proposed moving mesh finite difference method is considerably more efficient than the numerical methods offered in the literature.

KEYWORDS:
advection-diffusion, Dirichlet boundary condition, boundary layer, moving mesh, adaptivity, stability

1 | INTRODUCTION

The partial differentials are the ultimate essentials of physical problems in physics and engineering models. Solving partial differential equations (PDEs) analytically is a significant challenge for scientists; however, numerical solution of PDEs can obtain using finite difference and finite element method or other higher order numerical techniques. Mesh refinement techniques like domain decomposition and local refinement are employed to bring more accurate solutions, but these techniques can increase the computation cost and complexity. Moreover, the mesh refinement techniques using the hp-adaptive methods don't adjust according to the problem, especially near edges. The idea of the r-adaptive mesh refinement technique uses a much smaller number of mesh points than fixed mesh techniques. The MM-method is a sort of adaptive mesh method which moves nodes continuously in time. This magnificent idea of the adaptive moving mesh method introduced by Huang and Russell[26,30], we employ this method to deal with the advection-diffusion equation. The moving mesh finite difference method (MMFDM) utilizes time-dependent higher-order polynomials which give improved computational accuracy and efficiency. The adaptive moving mesh method is utilized successfully to determine solutions to several problems with high order accuracy[1,3,26]. Consider one dimensional linear advection diffusion equation:

$$\frac{\partial u}{\partial t} + c\frac{\partial u}{\partial x} = \nu\frac{\partial^2 u}{\partial x^2}, \quad 0 < x < L, \quad t \in (0, T] \tag{1}$$

The linear advection-diffusion equation oversees many extensive physics and engineering problems. It also aids in the application of Navier-Stokes equations[4,14,22]. In the fluids transport phenomenon, advection-diffusion occurs in oceanography physical processes occur. We consider a one-dimensional linear advection-diffusion equation with Dirichlet boundary conditions $u(t, x_o) = u\left(t, x_L\right) = 0$. We also observe that the (1) from its advection and diffusion terms that when the diffusion term dominates, the (1) becomes parabolic or when the advection term dominates, and the (1) becomes hyperbolic. The denomination of the advection term in (1), the solution becomes ill-behaving and difficult to obtain. From the literature, it is learned that scientists have presented numerous discretization techniques to obtain stable, efficient numerical schemes. In[15] extended cubic B-spline Galerkin arrangement in combination with the second-order Crank-Nicolson central difference scheme is used to solve the 1D LAD equation; however, it experiences the oscillations. In recent years B-splines have gotten a lot of attention from researchers to produce accurate results[13,17]; these splines are complicated. Several authors have solved the LAD problem analytically and numerically. Mojtabi et. al.[2] presented an analytical solution by making the change of variables as $u(t, x) = v(t, x)e^{\alpha x+\beta t}$ with which advection term is made to zero and a closed-form solution is presented with the aid of Fourier. Watkins et al. in[11] presented a nodal Discontinuous Galerkin approach via flux reconstruction solving LAD equation. The main goal of our work is to give high accuracy moving mesh FDM solution of linear advection-diffusion equation using Dirichlet boundary conditions. The organization of our work is hereafter: The first section elaborates on the analytical solution over the finite domain. Section 2 elaborates the series solution of the LAD equation using appropriate transformations. Section 3 an adaptive mesh finite difference method is described for the LAD equation. Section 4 elaborates on the mesh density functions and moving mesh PDEs. Section 5 presents the stability and convergence results and Section 6 demonstrates numerical results computed using the moving mesh finite difference semi-discretization scheme. The last section 7 concludes the remarks.

2 | THE TRANSPORT DIFFUSION EQUATION

Recalling the linear advection-diffusion equation in its unsteady form as:

$$\frac{\partial u}{\partial t} + c\frac{\partial u}{\partial x} = \nu\frac{\partial^2 u}{\partial x^2}, \quad -1 < x < 1, \quad t \in (0, T] \tag{2}$$

Where, $u(t, x)$ is the velocity, the advection velocity coefficient is $c > 0$, ν is kinematic viscosity, and t is time. The Dirichlet boundary conditions are $u(t, -1) = u(t, 1) = 0$, and the generic form of the initial condition: $u(0, x) = f(x)$ is imposed. With the aid of variable transformation, we can have a closed-form solution of the LAD equation[2]:

$$u(t, x) = v(t, x)e^{\alpha x+\beta t} \tag{3}$$

By inserting (3) in (2), one can have:

$$\frac{\partial v}{\partial t} + \left(\beta + c\alpha - \alpha^2 v\right) v + (c - 2\alpha v)\frac{\partial v}{\partial x} = v\frac{\partial^2 v}{\partial x^2} \tag{4}$$

With the appropriate selection of α and β, (4) can reduce to the standard heat equation:

$$\frac{\partial v}{\partial t} = v\frac{\partial^2 v}{\partial x^2} \tag{5}$$

The boundary conditions reduces to $v(t, -1) = v(t, 1) = 0$, and the non-homogeneous initial condition reduces to: $v(0, x) = -\sin(\pi x)e^{-\frac{cx}{2v}}$. The solution presented for the above-reduced problem in the Fourier series with the aid of separating variables. The exact solution is taken from the literature as[2]:

$$u(t, x) = 16\pi^2 v^3 c e^{\frac{c}{2v}\left(x-\frac{c}{2}t\right)}\left[G(t, x) + H(t, x)\right] \tag{6}$$

where,

$$G(t, x) = \sinh\left(\frac{c}{2v}\right)\sum_{p=0}^{\infty}\frac{(-1)^p 2p\sin(p\pi x)e^{-vp^2\pi^2 t}}{c^4 + 8(c\pi v)^2\left(p^2+1\right) + 16(\pi v)^4\left(p^2-1\right)^2}$$

and,

$$H(t, x) = \cosh\left(\frac{c}{2v}\right)\sum_{p=0}^{\infty}\frac{(-1)^p(2p+1)\cos\left(\frac{2p+1}{2}\pi x\right)e^{-v\frac{(2p+1)^2}{4}\pi t}}{^4 + (c\pi v)^2\left(8p^2+8p+10\right) + (\pi v)^4\left(4p^2+4p-3\right)^2}$$

We utilize the exact solution in (6) for the numerical solution validation and error measure in the L2-norm. Using conventional difference schemes is not accurate due to oscillatory behaviour of the concerned problem. We consider a complex but highly

efficient numerical method[25,27,28,29] to evaluate the LAD equation. Many authors have proposed a numerical solution to the LAD equation. Szymkiewicz presented a numerical solution if the 1D LAD equation used the process-splitting technique and a spline function for interpolation[18]. In[8], Karahan proposed the numerical solution of 1D ADE with a finite difference method using implicit spreadsheet simulation. In[20], S. Ortleb proposed fully discrete L^2 stability analysis for linear advection-diffusion equation, and the discontinuous Galerkin method based on diffusion schemes used to discretize in space. J. Lou et al. in[12] proposed a reconstructed discontinuous Galerkin (rDG) approach to evaluate the LAD equation on hybrid unconstructed grids.

3 | MOVING MESH PDES AND MESH DENSITY FUNCTIONS

$$\text{MMPDE4}: \quad \left(M x_{t,\xi}\right)_{\xi} = -\frac{1}{\tau}\left(M x_{\xi}\right)_{\xi} \tag{7}$$

$$\text{MMPDE5}: \quad x_t = \frac{1}{\tau}\left(M x_{\xi}\right)_{\xi} \tag{8}$$

$$\text{ModifiedMMPDE5}: \quad x_t = \frac{1}{M\tau}\left(M x_{\xi}\right)_{\xi} \tag{9}$$

$$\text{MMPDE6}: \quad x_{t,\xi\xi} = -\frac{1}{\tau}\left(M x_{\xi}\right)_{\xi} \tag{10}$$

where $M = M(t, x)$ is the mesh density function. In MMPDEs, the term $\tau > 0$ is responsible for the mesh displacement. The minor the value of τ, the more rapidly mesh reacts to the variate in $M(x, t)$. In the literature, the arc-length and the curvature mesh density functions are the most commonly encountered mesh density functions (MDF).

$$\text{arc}-\text{length}: \quad M(t,x) = \sqrt{1+\alpha u_x^2} \tag{11}$$

$$\text{curvature}: \quad M(t,x) = \left(\alpha + \beta u_{xx}^2\right), \text{ where } n = 2 \text{ or } n = 4 \tag{12}$$

α and β are the adaptive parameters[7,31], which can be picked according to problem dynamics. The preference for mesh density function is the principle in mesh movement. The MDF decides the allocation of mesh points in the neighborhood of the domain.

4 | MOVING MESH SEMI-DISCRETIZATION FINITE DIFFERENCE SCHEME

The numerical solution of the linear advection-diffusion equation using the adaptive moving mesh finite difference method will present in this section. We define coordinate transformation as:

$$x = x(\xi, t) : \xi \in \Omega_c \equiv [-1, 1] \to x \in \Omega_p \equiv (a, b),\ t > 0 \tag{13}$$

where x and ξ represents the space variables, t is time. Ω_c represents the computational domain and Ω_p resents physical domain. The coordinate transformation from a physical domain to a computational domain is employed; using the chain rule:

$$u_t = \dot{u} - \dot{x}u_x, \quad u_x = \frac{u_\xi}{x_\xi}, \quad u_{xx} = \frac{1}{x_\xi}\left(\frac{u_\xi}{x_\xi}\right)_\xi \tag{14}$$

Use the above definitions, (2) becomes as:

$$\dot{u} - \dot{x}\frac{u_\xi}{x_\xi} + c\frac{u_\xi}{x_\xi} = \frac{\nu}{x_\xi}\left(\frac{u_\xi}{x_\xi}\right)_\xi \tag{15}$$

Then yields,

$$(\dot{x_\xi u}) - \dot{x}_\xi u - (\dot{x} - c)\, u_\xi = \nu\left(\frac{u_\xi}{x_\xi}\right)_\xi = 0 \tag{16}$$

A fixed uniform mesh is defined using the equidistribution principle on the computational domain as Ω_c as: $\mathcal{T}_h^n : \xi_j = \frac{j-1}{N-1}, j = 1, \ldots, N$.

$$\xi_k = \frac{k}{M}, \quad k = 0, 1, \ldots, M. \tag{17}$$

Then a time-dependent mesh is given by:

$$x_k(\tau) = x(\xi_k, \tau) = x(k/M, \tau), \quad k = 0, 1, \ldots, M. \tag{18}$$

The degree of each physical cell can be imply as:

$$h_k(\tau) = x_k(\tau) - x_{k-1}(\tau), \quad k = 0, 1, \ldots, M. \tag{19}$$

The midpoints of the cells can be defined as:

$$x_{k-1/2}(t_m) = \frac{1}{2}\left(x_k(t_m) + x_{k-1}(t_m)\right), \quad k = 0, 1, \ldots, M. \tag{20}$$

Considering $x^h(\xi, t)$ is piecewise-quadratic in space and linear in time, such that:

$$x^h(\xi, t_m) = x_{k-1/2}(t_m)\ell_0(\xi) + x_k(t_m)\ell_1(\xi) + x_{k+1/2}(t_m)\ell_2(\xi). \tag{21}$$

where ℓ_0, ℓ_1, ℓ_2 are quadratic Lagrange polynomials, then for $\xi_{k-1/2} \le \xi \le \xi_{k+1/2}$,

$$x^h(\xi, t) = x^h(\xi, t_m) + (t - t_m)\frac{x^h(\xi, t_{m+1}) - x^h(\xi, t_m)}{t_{m+1} - t_m}. \tag{22}$$

then we can have,

$$\left(\dot{x}^h_\xi\right)^{m+1}_k = \frac{\left(x^h_\xi\right)^{m+1}_k - \left(x^h_\xi\right)^m_k}{t_{m+1} - t_m} = \frac{\dot{x}^h\left(\xi_{k+1/2}, t_{m+1}\right) - \dot{x}^h\left(\xi_{k-1/2}, t_{m+1}\right)}{\Delta\xi}. \tag{23}$$

and

$$x^h_\xi\left(t_m\right) = \frac{x_{k+1/2}\left(\tau_m\right) - x_{k-1/2}\left(t_m\right)}{\Delta\xi} = \frac{1}{\Delta\xi}\left(\frac{h^m_{k+1} + h^m_k}{2}\right), \quad \xi_{k-1/2} < \xi < \xi_{k+1/2}. \tag{24}$$

With the above-defined equality, we see that $x^h(\xi, t)$ satisfies a discrete geometric conservation law.

$$\left(x^h_\xi\right)^{m+1}_k = \left(S^h_\xi\right)^m_k + \frac{t_{m+1} - t_m}{\Delta\xi}\left(\dot{x}^h_{k+1/2} - \dot{x}^h_{k-1/2}\right). \tag{25}$$

Now derive the semi-discretization scheme for (16), using the notation V^m_k for the approximate solution of $C(S^m_k, \tau_m)$. The backward and forward divided differences can define as:

$$(D_+V)_k = \frac{V_{k+1} - V_k}{h_k}, \quad (D_-V)_k = \frac{V_k - V_k}{h_{k-1}}. \tag{26}$$

and the average operator can be given as:

$$(\delta V)_{k+1/2} = \frac{1}{2}\left(V_k + V_{k+1}\right). \tag{27}$$

Employ Central Difference for spatial and Backward Euler for temporal derivatives in (16),

$$\begin{aligned}(\dot{x_\xi u}) - \dot{x}_\xi u - (\dot{x} - c)\, u_\xi - \nu\left(\frac{u_\xi}{x_\xi}\right)_\xi \approx \frac{\left(x^h_\xi V\right)^{m+1}_k - \left(x^h_\xi V\right)^m_k}{\Delta\tau_{m+1}} - (\dot{x})^{m+1}_j V^{m+1}_k \\ -\frac{1}{2\Delta\xi}\left[\left(\nu\left(D_+ - D_-\right)V\right)^{m+1}_k - \left(\left(\dot{x^h}\right)^{m+1}_k - c\right)\left((\delta V)^{m+1}_{j+1/2} - (\delta V)^{m+1}_{j-1/2}\right)\right].\end{aligned} \tag{28}$$

Such that, we have obtained a numerical scheme for (16):

$$\begin{aligned}\left(x^h_\xi V\right)^{m+1}_k = \left(x^h_\xi V\right)^m_k - \Delta\tau\,(\dot{x})^{m+1}_j V^{m+1}_k \\ -\frac{1}{2\Delta\xi}\left[\left(\nu\left(D_+ - D_-\right)V\right)^{m+1}_k - \left(\left(\dot{x^h}\right)^{m+1}_k - c\right)\left((\delta V)^{m+1}_{j+1/2} - (\delta V)^{m+1}_{j-1/2}\right)\right].\end{aligned} \tag{29}$$

The stability and convergence results will figure out in the next section.

5 | STABILITY AND CONVERGENCE

The mesh dependent L_2 norm can be defined as:

$$\|V\|_n = \left(\sum_{j=1}^{M-1}\left(\frac{h^m_k + h^m_{k+1}}{2}\right)\left(V_j\right)^2\right)^{\frac{1}{2}}. \tag{30}$$

and the differentials can be estimated using cell-based norms:

$$\|W\|_{\bar{m}} = \left(\sum_{k=1}^{M-1} h^m_k\left(W_j\right)^2\right)^{\frac{1}{2}}. \tag{31}$$

Theorem 1. Consider the scheme (28) is adopted for the formulation of (16), then sufficiently small mesh intervals, a priori bound may persist:

$$\|V^{m+1}\|_{m+1} \leq A\|V^0\|_0. \tag{32}$$

where A is a universal constant.

Proof. Multiply V_k^{m+1} on both sides of expression (29) and sum all the interior nodes (since $V_0 = V_M = 0$), we get:

$$\sum_{k=1}^{M-1} \left(x_\xi^h\right)_k^{m+1} \left(V_j^{m+1}\right)^2 = \mathbf{I} + \mathbf{II} + \mathbf{III} + \mathbf{IV}. \tag{33}$$

where

$$\mathbf{I} = \sum_{k=1}^{M-1} \left(x_\xi^h\right)_k^m V_k^m V_k^{m+1},$$

$$\mathbf{II} = \Delta t_{m+1} \sum_{k=1}^{M-1} \left(\dot{x_h}\right)_k^{m+1} \left(V_k^{m+1}\right)^2, \tag{34}$$

$$\mathbf{III} = \frac{\nu \Delta t_{m+1}}{2\Delta\xi} \sum_{k=1}^{M-1} \left[\left(\left(D_+ - D_-\right) V\right)_k^{m+1}\right] V_k^{m+1}, \tag{35}$$

$$\mathbf{IV} = \frac{\Delta t_{m+1}}{\Delta\xi} \sum_{k=1}^{M-1} \left[\left(\dot{x^h} - c\right)_k^{m+1} \left((\delta V)_{k+1/2}^{m+1} - (\delta V)_{k-1/2}^{m+1}\right)\right] V_k^{m+1}. \tag{36}$$

Exercising the argument in (26), (27) and employing the identity:

$$ab = \frac{1}{2}a^2 + \frac{1}{2}b^2 - \frac{1}{2}(a-b)^2.$$

then,

$$\mathbf{I} = \frac{1}{2} \sum_{k=1}^{M-1} \left(x_\xi^h\right)_k^m \left[\left(V_k^{m+1}\right)^2 + \left(V_k^m\right)^2 - \left(V_k^{m+1} - V_k^m\right)^2\right],$$

$$\mathbf{I} = \frac{1}{2} \sum_{k=1}^{M-1} \left(x_\xi^h\right)_k^m \left(V_k^{m+1}\right)^2 + \frac{1}{2} \sum_{k=1}^{M-1} \left(x_\xi^h\right)_k^m \left(V_k^m\right)^2 - \frac{1}{2} \sum_{k=1}^{M-1} \left(x_\xi^h\right)_k^m \left(V_k^{m+1} - V_k^m\right)^2,$$

using (23),(24) and (26), such that

$$\mathbf{I} = \frac{1}{2} \sum_{k=1}^{M-1} \left[\left(x_\xi^h\right)_k^{m+1} \left(V_k^{m+1}\right)^2 - \frac{\Delta t_{m+1}}{2\Delta\xi} \sum_{k=1}^{M-1} \left(\left(\dot{x^h}\right)_{k+1/2}^{m+1} - \left(\dot{S^h}\right)_{k-1/2}^{m+1}\right)\right]$$
$$+ \frac{1}{2} \sum_{k=1}^{M-1} \left[\left(x_\xi^h\right)_k^m \left(V_k^m\right)^2 - \left(x_\xi^h\right)_k^m \left(V_k^{m+1} - V_k^m\right)^2\right],$$

$$\mathbf{I} \leq \frac{1}{2\Delta\xi} \left(\|V^{m+1}\|_{m+1}^2 + \|V^m\|_m^2\| - \|V^{m+1} - Vm\|_m^2\|\right) + A\frac{\Delta t_{m+1}}{\Delta\xi}\|V^{m+1}\|_{m+1}^2. \tag{37}$$

Utilizing the same reasoning as in[9], we have beginequation

$$\mathbf{II} = -\frac{\nu \Delta t_{m+1}}{2\Delta\xi}\|D_+ V^{m+1}\|_{\bar{m+1}}^2. \tag{38}$$

Utilizing (23), as:

$$\mathbf{III} = \frac{\Delta t_{m+1}}{\Delta\xi} \sum_{k=1}^{M-1} \left(\dot{x}_{j+1/2}^{m+1} - \dot{x}_{j-1/2}^{m+1}\right) \left(V_k^{m+1}\right)^2 \leq A\frac{\Delta t_{m+1}}{\Delta\xi}\|V^{m+1}\|_{m+1}^2 \tag{39}$$

We have $V_0^{m+1} = V_M^{m+1} = 0$, such that

$$\begin{aligned}
\mathbf{IV} &= \frac{\Delta t_{m+1}}{2\Delta\xi} \sum_{k=1}^{M-1} \left[\left(\dot{x}^h - c\right)_k^{m+1} V_{k+1}^{m+1} V_k^{m+1} - \left(\dot{x}^h - c\right)_k^{m+1} V_k^{m+1} V_{k-1}^{m+1} \right] \\
&= \frac{\Delta t_{m+1}}{2\Delta\xi} \left[\sum_{k=1}^{M-1} \left[\left(\dot{x}^h - c\right)_k^{m+1} V_{k+1}^{m+1} V_k^{m+1} \right] - \sum_{k=1}^{M-2} \left[\left(\dot{x}^h - c\right)_{k+1}^{m+1} V_{k+1}^{m+1} V_k^{m+1} \right] \right] \\
&\leq \frac{\Delta t_{n+1}}{4\Delta\xi} \sum_{j=1}^{N-2} \left[\left(\dot{x}^h\right)_{j+1}^{n+1} - \left(\dot{x}^h\right)_j^{n+1} \right] \left[\left(V_{j+1}^{n+1}\right)^2 + \left(V_j^{n+1}\right)^2 \right] \\
&\leq A \frac{\Delta t_{m+1}}{\Delta\xi} \|V^{m+1}\|_{m+1}^2.
\end{aligned} \tag{40}$$

Incorporate estimations (37), (38), (39) and (5.8) in (33), we have:

$$\begin{aligned}
\left\|V^{m+1}\right\|_{m+1}^2 \leq &\left(\|V^m\|_m^2 - \left\|V^{m+1} - V^m\right\|_m^2 \right) - 2\nu\Delta t_{m+1} \left\|D_+ V^{m+1}\right\|_{m+1}^2 \\
&+ A\Delta t_{m+1} \left\|V^{m+1}\right\|_{m+1}^2
\end{aligned} \tag{41}$$

Such that,

$$\left\|V^{\ell+1}\right\|_{\ell+1}^2 \leq \left\|V^{\ell}\right\|_{\ell}^2 + A\Delta t_{\ell+1} \left\|V^{\ell+1}\right\|_{\ell+1}^2 \tag{42}$$

Lets sum (42) for $\ell = 0, 1, ..., N$, we will get:

$$\left\|V^{N+1}\right\|_{\ell+1}^2 \leq \left\|V^{\ell}\right\|_0^2 + A\Delta t_{\ell+1} \left\|V^{\ell+1}\right\|_{\ell+1}^2 \tag{43}$$

$$\left\|U^{M+1}\right\|_{M+1}^2 \leq \frac{\|V^0\|_0^2}{1 - A\Delta t_{M+1}} + \frac{A}{1 - A\Delta t_{M+1}} \sum_{\ell=1}^{M} \Delta t_\ell \left\|V^{\ell}\right\|_{\ell}^2. \tag{44}$$

The equidistribution principle can be defined as:

$$\int_{x_k^m}^{x_{k+1}^m} M(x,t)dx = \frac{1}{M} \int_{x_L}^{x_R} M(x,t)dx, \quad k = 0, ..., N, \quad m = 1, ..., L$$

The monitor function $M(x,t) > 1$, such that

$$\int_{x_k^m}^{x_{k+1}^m} M(x,t) \leq A$$

Similarly, we have

$$h_k^m \equiv x_{k+1}^m - x_k^m \leq \int_{x_k^m}^{x_{k+1}^m} M(x,t)dx \tag{45}$$

$$= \frac{1}{M} \int_{x_L}^{x_R} M(x,t)dx \leq \frac{A}{M} \tag{46}$$

From [10] and [9], we induce that while scheme (28) is employed to (2) the error will have the bound as:

$$\left\|e^0\right\|_0^2 \leq A \left[\max\left(t, M^{-2}\right)\right]^2 \tag{47}$$

□

Numerical validation will present in the next section. We will employ four MMPDEs (i.e., MMPDE4, MMPDE5, modified MMPDE5, MMPDE6) with varying the number of nodes. A weighted averaging is suggested by Huang et al. for smooth mesh

movement[27,28].

$$\hat{\rho}_j := \sqrt{\frac{\sum_{k=j-p}^{j+p} \hat{\rho}_k^2 \left(\frac{\gamma}{1+\gamma}\right)^{|k-j|}}{\sum_{k=j-p}^{j+p} \left(\frac{\gamma}{1+\gamma}\right)^{|k-j|}}}, j = 1, \ldots, M+1 \tag{48}$$

where p is called the smoothing index, a non-negative integer, and γ is the positive smoothing parameter.

6 | NUMERICAL EXPERIMENTS AND DISCUSSION

In this section, numerical results are obtained with four MMPDEs and with a varying number of nodes. We perform the numerical experiments for the 1D linear advection-diffusion equation with Dirichlet boundary conditions. We consider five cases for the Reynolds number; three are periodic Reynolds numbers. The numerical solution is obtained with a different number of mesh points, i.e., 200, 400, 600, 800, and 1200. We have compared the numerical solutions with the analytical solution in (6), proposed by Mojabi et al.[2]. The accomplished numerical solution using one-dimensional homogeneous boundary conditions with the sinusoidal initial condition; the fixed boundary can be seen in the Figure 1, for $t > 0$, with increasing time, the variation moves towards the terminal boundary. If the Reynolds number is infinite, we will have a shock wave at the boundary. At a high Reynolds number, the flow will hit the boundary at $x = 1$. The mesh time response coefficient is taken as $\tau = 10^{-4}$. The maximum absolute error can approximate using the L2-norm. Reynolds number can be defined as $Re = \frac{cL}{\nu}$, choosing $L = 2$ and $c = 1$ for the solutions, and the Reynolds number can reduce as $Re = \frac{2}{\nu}$.

Example 2 (Case I)**.** For, $Re = 20\pi$, $\upsilon = \frac{1}{10\pi}$

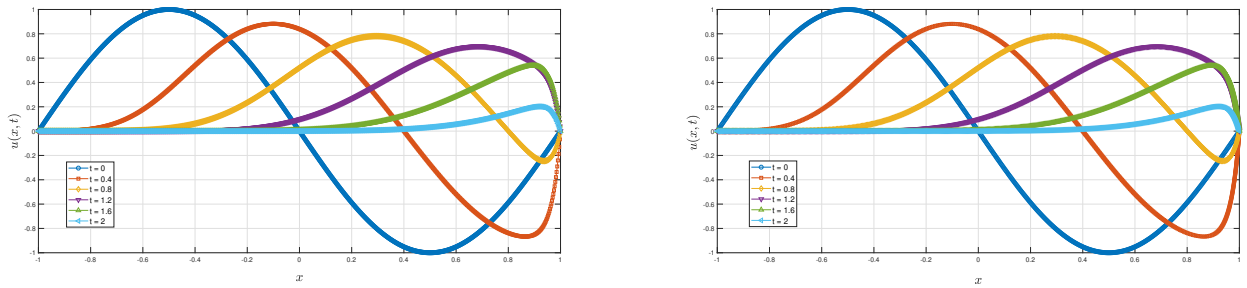

Figure 1 Analytical and numerical solution for different times varying from $t = 0$ to $t = 2.0$, using $Re = 20\pi$. The approximate solution is obtained with $N = 800$.

TABLE 1 *The maximum error measure is obtained using the exact solution and the approximate solution. The approximate solution is attained using four MMPDEs with varying number of mesh points. We observe that the error measured is the order of* 10^{-5} *in comparison with fixed mesh the order is* 10^{-3}.

	Maximum Error Estimate				
$N \rightarrow$	200	400	600	800	1200
MMPDE4	8.03e − 002	3.71e − 002	7.38e − 003	9.10e − 005	4.66e − 007
MMPDE5	7.66e − 002	3.21e − 002	6.59e − 003	8.18e − 005	4.21e − 006
MMPDE6	1.52e − 002	1.05e − 002	6.81e − 004	8.38e − 005	4.45e − 006
modified MMPDE5	7.67e − 002	1.91e − 002	2.87e − 003	9.00e − 005	4.38e − 007
MMPDE6	7.67e − 002	1.91e − 002	2.87e − 003	9.00e − 005	4.38e − 007
Fixed mesh	1.96e − 002	1.02e − 002	9.83e − 003	4.28e − 003	1.92e − 003

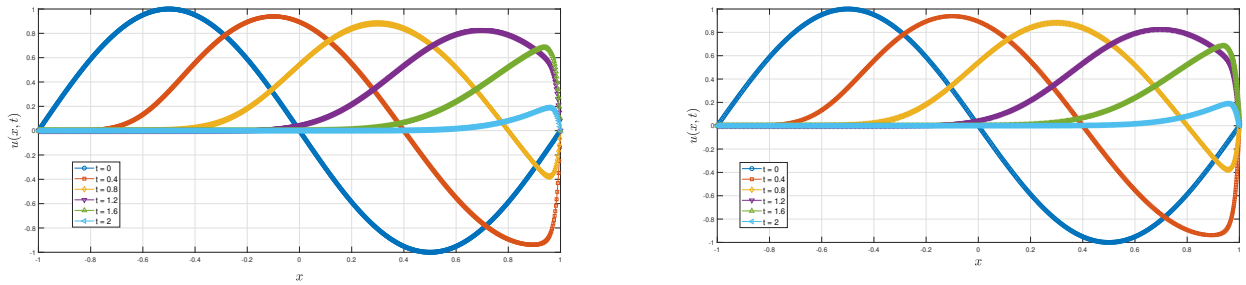

Figure 2 Analytical and numerical solution for different times varying from $t = 0$ to $t = 2.0$, using $Re = 40\pi$. The approximate solution is obtained with $N = 800$.

We observe from the Figure 1, that with $Re = 20$ boundary layer accelerate towards the boundary $x = 1$ with increasing time. The arc-length mesh density function with MMPDE4 is employed to obtain the numerical approximation. The analytical solution is shown in the left of Figure 1. From the Table 1, we observe that error reduces with the increasing N, and the solution converges with the increasing number of mesh points.

Example 3 (Case II)**.** For, $Re = 40\pi,\ \upsilon = \frac{1}{20\pi}$

TABLE 2 *The maximum error measure is obtained using the exact solution and the approximate solution. The approximate solution is attained using four MMPDEs with varying numbers of mesh points. We observe that the error measured is the order of* 10^{-5} *in comparison with fixed mesh the order is* 10^{-3}.

	Maximum Error Estimate				
$N \rightarrow$	200	400	600	800	1200
MMPDE4	4.71e − 002	9.95e − 003	9.67e − 004	5.84e − 005	3.32e − 007
MMPDE5	4.41e − 002	9.45e − 003	8.66e − 004	5.25e − 005	3.00e − 007
MMPDE6	4.48e − 002	9.13e − 003	8.44e − 004	4.89e − 005	2.89e − 007
modified MMPDE5	2.92e − 002	9.19e − 003	8.92e − 004	5.85e − 005	4.34e − 007
Fixed mesh	1.40e − 001	1.65e − 002	8.60e − 003	4.37e − 003	4.12e − 004

Figure 2 shows the numerical and analytical solutions of the LAD equation using $Re = 40\pi$ and $c = 1$. We can observe from Figure 2 that the boundary layer is descending with time as the Reynolds number is periodic. We observe from Table 2 that the solution converges as the error reduces with the increasing number of nodes. Figure 4 shows that the solution's boundary layer does not decay with time because the Reynolds number is not periodic. We have used the arc-length monitor function with different MMPDEs to obtain the approximate solution demonstrated in Table 3; we observe that the error is scaling down with the increasing number of mesh points. Figure 3 shows the numerical and analytical solutions with $Re = 200\pi$. Table 5 and Figure 5 are obtained with speed $c = 1$ and Reynolds number $Re = 4000$.

Example 4 (Case III)**.** For, $Re = 2000,\ \upsilon = \frac{1}{1000}$

Example 5 (Case IV)**.** For, $Re = 200\pi,\ \upsilon = \frac{1}{100\pi}$

In Table 5 and Figure 6 are obtained with speed $c = 1$ and Reynolds number $Re = 4000$.

Example 6 (Case V)**.** For, $Re = 2000,\ \upsilon = \frac{1}{2000}$

In Figure 6, we observe that mesh points are concentrated near the leading and trailing edges. The increased number of points are redistributed in the region of edges, this enables the accuracy of the approximate solution. The solution in Figure 6, we have used speed $c = 2$, we can see that flow for time $t = 0, 0.4, 0.8$ are starting before the second boundary. But for time $t = 1.2, 1.6$, and 2.0 didn't start before striking the wall at $x = 1$. The numerical solution is approximated using four MMPDEs with varying numbers of mesh points. We observe that the error measured is the order of 10^{-5} in comparison with fixed mesh the order is 10^{-3}. Analytical and numerical solution for different times varying from $t = 0$ to $t = 2.0$, using $Re = 200\pi$. The approximate

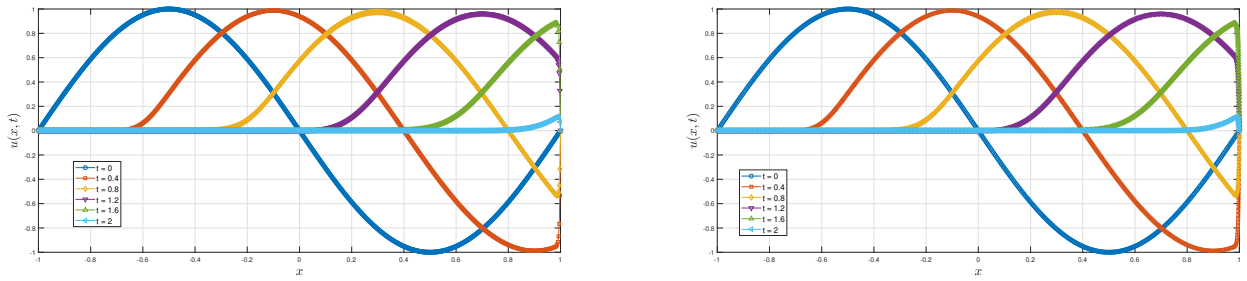

Figure 3 Analytical and numerical solution for different times varying from $t = 0$ to $t = 2.0$, using $Re = 200\pi$. The approximate solution is obtained with $N = 800$.

Table 3 The maximum error measure is obtained using the exact solution and the approximate solution. The approximate solution is attained using four MMPDEs with varying numbers of mesh points. We observe that the error measured is the order of 10^{-5} in comparison with fixed mesh the order is 10^{-3}.

	Maximum Error Estimate				
$N \rightarrow$	200	400	600	800	1200
MMPDE4	8.09e − 002	5.22e − 002	1.07e − 003	5.47e − 005	9.81e − 007
MMPDE5	7.72e − 002	4.81e − 002	9.91e − 004	5.16e − 005	1.01e − 006
MMPDE6	1.57e − 002	2.31e − 002	6.64e − 004	3.60e − 005	2.45e − 006
modified MMPDE5	7.77e − 002	4.66e − 002	1.01e − 003	3.64e − 005	8.94e − 007
Fixed mesh	8.54e − 002	5.20e − 002	5.20e − 002	9.82e − 003	6.57e − 003

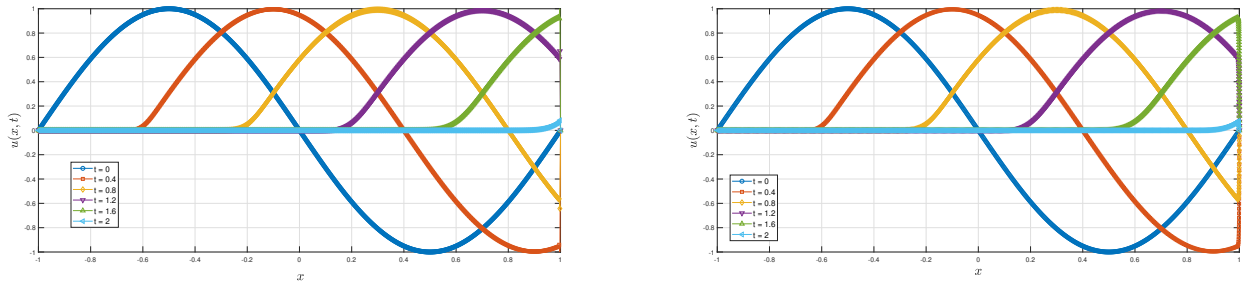

Figure 4 Analytical and numerical solution for different times varying from $t = 0$ to $t = 2.0$, using $Re = 2000$. The approximate solution is obtained with $N = 800$.

Table 4 The maximum error measure is obtained using the exact solution, with the approximate solution obtained employing four MMPDEs and the different mesh points. The table shows that the error measured with adaptive mesh is in the order of $10 - 5$ compared to $10 - 3$ with fixed mesh.

	Maximum Error Estimate				
$N \rightarrow$	200	400	600	800	1200
MMPDE4	5.30 − 002	9.57e − 003	2.22e − 003	5.15e − 004	2.66e − 006
MMPDE5	4.96e − 002	8.62e − 003	2.86e − 003	7.15e − 005	1.73e − 006
MMPDE6	4.48e − 002	1.06e − 002	8.74e − 004	5.48e − 005	2.82e − 006
modified MMPDE5	5.02e − 002	9.57e − 002	4.24e − 004	1.71e − 004	1.03e − 006
Fixed mesh	6.14e − 002	3.29e − 002	1.98e − 002	8.60e − 003	4.73e − 003

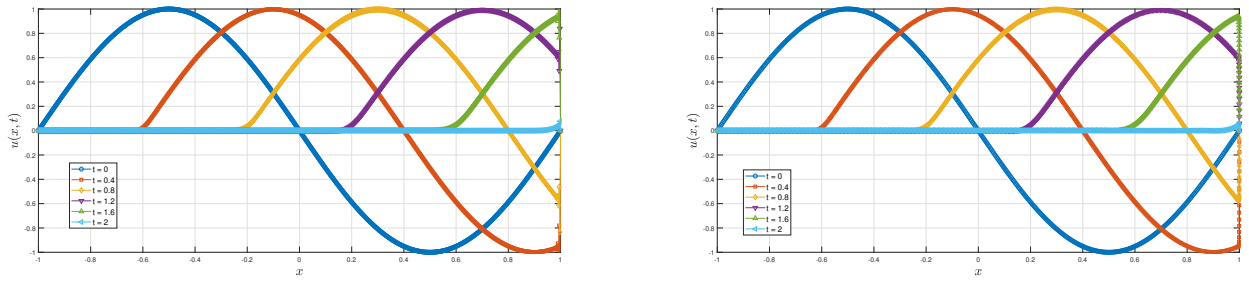

Figure 5 Analytical and numerical solution for different times varying from $t = 0$ to $t = 2.0$, using $Re = 4000$. The approximate solution is obtained with $N = 800$.

Table 5 The maximum error measure is obtained using the exact solution with the numerical solution obtained using four MMPDEs and the different mesh points. We can see from the table that the error measured with moving mesh is the order of 10^{-5} in comparison with fixed mesh is 10^{-3}.

	Maximum Error Estimate				
$N \rightarrow$	200	400	600	800	1200
MMPDE4	3.35e − 002	1.50e − 003	1.87e − 004	8.84e − 006	2.41e − 007
MMPDE5	3.43e − 002	1.42e − 003	1.52e − 004	9.75e − 006	3.50e − 007
MMPDE6	3.42e − 002	1.93e − 003	–	–	–
modified MMPDE5	4.51e − 002	6.30e − 004	1.95e − 005	8.84e − 006	8.16e − 007
Fixed mesh	7.17e − 002	5.72e − 002	2.79e − 002	7.53e − 003	6.30e − 003

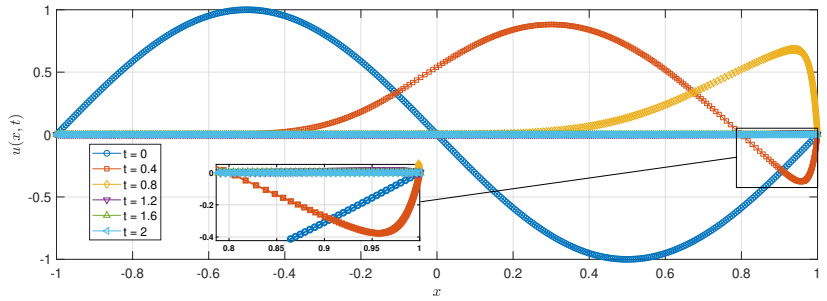

Figure 6 The sharp edge in the numerical solution is zoomed to observe that mesh is moving accurately.

solution for all the cases are obtained with $N = 800$. The numerical experiments were performed using MATLAB built-in fully implicit ordinary differential equations solver $ODE15i$. We use three kinds of mesh density functions (i.e., piecewise linear approximations, arc-length, and curvature). While evaluating the results, we have seen that arc length was the best in handling integration tolerances of the equation. With other mesh density functions, the subject equation sometimes becomes stiffer. In case III and case V, the arc-length mesh density function wasn't effective with an increased number of nodes; we have utilized piecewise linear approximation for this case. For $Re = 4000$, with MMPDE6 and $N > 500$ the program is unable to meet the integration tolerances. The approximate solution is approximated using four MMPDEs with varying numbers of mesh points. We observe that the error measured is the order of 10^{-5} in comparison with fixed mesh the order is 10^{-3}. Analytical and numerical solution for different times varying from $t = 0$ to $t = 2.0$, using $Re = 200\pi$. The approximate solution for all the cases are obtained with $N = 800$. The numerical experiments were performed using MATLAB built-in fully implicit ordinary differential equations solver $ODE15i$. We use three kinds of mesh density functions (i.e., piecewise linear approximations, arc-length, and curvature). While evaluating the results, we have seen that arc length was the best in handling integration tolerances of the

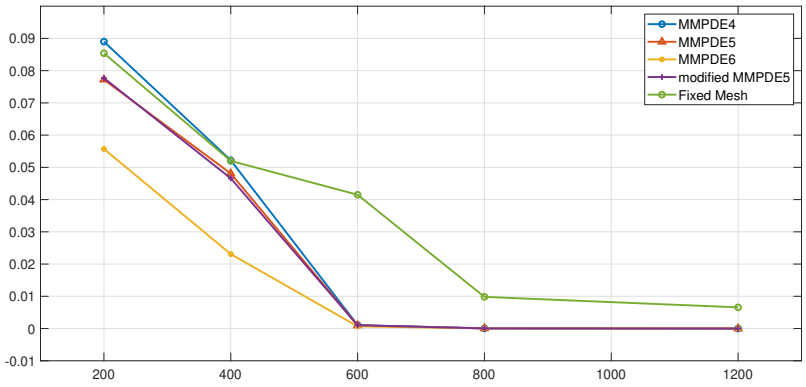

Figure 7 Maximum absolute error estimate for the Re.2000, error is plotted for different MMPDEs against the number of mesh points.

equation. With other mesh density functions, the subject equation sometimes becomes stiffer. In case III and case V, the arc-length mesh density function wasn't effective with an increased number of nodes; we have utilized piecewise linear approximation for this case. For $Re = 4000$, with MMPDE6 and $N > 500$ the program is unable to meet the integration tolerances.

7 | CONCLUSIONS

We have applied moving mesh method based on moving mesh PDEs and mesh density functions. Adaptive moving mesh method satisfyingly analyzed the boundary layer numerically with five cases of Reynolds numbers using the semi-discretization central difference scheme for space and Backward Euler for time derivatives. The numerical solution is compared with the analytical solution with varying numbers of mesh points. The maximum absolute error measure is compared for the different numbers of mesh points. We examine that the error measure for the adaptive moving mesh is consistently smaller than the stationary mesh. The adaptive moving mesh method successfully analyzes an efficient and accurate solution of the LAD equation compared with the solution obtained using stationary mesh. However, the moving mesh adaptive method takes more computation time due to the moving mesh PDEs that needs to solve along with the subject DE. Mesh density function have significant importance in the success of adaptive method and its selection is central in the accuracy of method. We observe that the arc-length mesh density function performed better than other density functions. We may extend this work to Neumann and mixed boundary conditions in the future.

References

1. Abdulghani Alharbi and Shailesh Naire An adaptive moving mesh method for thin film flow equations with surface tension, Journal of Computational and Applied Mathematics, 319 (2017) 365–384.

2. Abdelkader Mojtabi and Michel O. Deville, One-dimensional linear advection–diffusion equation: Analytical and finite element solutions, Computers and Fluids, 107 (2015) 189–195.

3. Alexander N. Brooks and Thomas J.R. Hughes, Streamline upwind/Petrov-Galerkin formulations for convection dominated flows with particular emphasis on the incompressible Navier-Stokes equations, Computer Methods in Applied Mechanics and Engineering, 32 (1982) 119–259.

4. Antti H. Niemi, Nathaniel O. Collier and Victor M. Calo, Discontinuous Petrov–Galerkin method based on the optimal test space norm for steady transport problems in one space dimension, Journal of Computational Science, 4 (2013) 157–163.

5. Chris J. Budd, Weizhang Huang and Robert D. Russell, Adaptivity with moving grids, Acta Numerica, 18 (2009) 111–241.

6. Daniela Buske, Bardo Bodmann, Marco T.M.B. Vilhena, Régis S.de Quadros, On the Solution of the Coupled Advection-Diffusion and Navier-Stokes Equations, American Journal of Environmental Engineering, 5 (2015) 1—8.

7. G. Beckett and J.A. Mackenzie, Convergence analysis of finite difference approximations on equidistributed grids to a singularly perturbed boundary value problem, Applied Numerical Mathematics, 35 (2000) 87–109.

8. Halil Karahan, Implicit finite difference techniques for the advection–diffusion equation using spreadsheets, Advances in Engineering Software, 37 (2006) 601–608.

9. J.A. Mackenzie and W. R. Mekwi, An analysis of stability and convergence of a finite-difference discretization of a model parabolic PDE in 1D using a moving mesh, IMA Journal of Numerical Analysis, 27:507-–528, Nov 2006.

10. Jingtang Ma, Yingjun Jiang and Kaili Xiang, On a moving mesh method for solving partial integro-differential equations, Journal of Computational Mathematics, 27:713–728, Nov 2009.

11. Jerry Watkins, Kartikey Asthana and Antony Jameson, A numerical analysis of the nodal Discontinuous Galerkin scheme via Flux Reconstruction for the advection-diffusion equation, Computers and Fluids, 139 (2016) 233—247.

12. Jialin Lou, Lingquan Li, Hong Luo and Hiroaki Nishikawa, Reconstructed discontinuous Galerkin methods for linear advection–diffusion equations based on first-order hyperbolic system, Journal of Computational Physics, 369 (2018) 103–124.

13. Joan Goh, Ahmad Abd. Majid and Ahmad Izani Md. Ismail, Cubic B-Spline Collocation Method for One-Dimensional Heat and Advection-Diffusion Equations, Journal of Applied Mathematics, 2012 (2012) 8.

14. Johnson Claes and Jukka Saranen, Streamline Diffusion Methods for the Incompressible Euler and Navier-Stokes Equations, American Mathematical Society: Mathematics of Computation, 47 (1986) 1–18.

15. M. Zorsahin Gorgulu, İ. Dag, S. Dogan and D. Irk, A NUMERICAL SOLUTION OF THE ADVECTION-DIFFUSION EQUATION BY USING EXTENDED CUBIC B-SPLINE FUNCTIONS, Anadolu University Journal of Science and Technology A - Applied Sciences and Engineerin, 19 (2018) 347–355.

16. Philip Gresho, David Griffiths and David Silvester, Adaptive Time-Stepping for Incompressible Flow Part I: Scalar Advection-Diffusion, SIAM Journal on Scientific Computing, 30 (2008) 6387—6417.

17. R.C. Mittal and R.K. Jain, Redefined cubic B-splines collocation method for solving convection–diffusion equations, Applied Mathematical Modelling, 36 (2012) 5555–5573.

18. R. Szymkiewicz , Solution of the advection–diffusion equation using the spline function and finite elements, Computer Methods in Applied Mechanics and Engineering, 32 (1982) 119–259.

19. S. Dhawan, S. Kapoor and S. Kumar, Numerical method for advection diffusion equation using FEM and B-splines, Journal of Computational Science, 3 (2012) 429—437.

20. Sigrun Ortleb, L2-stability analysis of IMEX-(σ, μ)DG schemes for linear advection-diffusion equations, Applied Numerical Mathematics, 147 (2020) 43–65.

21. Tang Tao, Moving mesh methods for computational fluid dynamics, Contemporary Mathematics, 383 (2005).

22. Thomsan J. W, Numerical Partial Differential Equations: Finite Difference Methods, Springer-Verlag, New York 1995.

23. Trung Vo-Duy, One Dimensional Burgers Equation, Department of Applied Mathematics, Gran Sasso Science Institute, L'aquila, Italy, 2018.

24. Weizhang Huang and Weiwei Sun, Variational mesh adaptation II: error estimates and monitor functions, Journal of Computational Physics, 184 (203) 619–648.

25. Weiming Cao, Weizhang Huang, and Robert D. Russell, A moving mesh method based on the geometric conservation law, SIAM Journal on Scientific Computing, 24 (1995), 118—142.

26. Weizhang Huang and Robert D. Russell, Adaptive mesh movement — the MMPDE approach and its applications, Journal of Computational and Applied Mathematics, 128 (2001) 383–398.

27. Weizhang Huang, Yuhe Ren and Robert D. Russell, Moving Mesh Methods Based on Moving Mesh Partial Differential Equations, Journal of Computational Physics, 113 (1994) 279–290.

28. Weizhang Huang, Yuhe Ren and Robert D. Russell, Moving mesh partial differential equations (mmpdes) based on the equidistribution principle, SIAM J. Numerical Analysis, 31 (1994) 709–730.

29. Weiming Cao, Weizhang Huang and Robert D. Russell, Approaches for generating moving adaptive meshes: location versus velocity, Applied Numerical Mathematics, 47 (2003) 121–138.

30. Weizhang Huang and Robert D. Russell, Adaptive Moving Mesh Methods, Springer, New York 2011.

31. Weizhang Huang and Robert D. Russell, Analysis of moving mesh partial differential equations with spatial smoothing, SIAM Journal on Numerical Analysis, 34 (2006) 1106—1126.

32. Yuchi Qiu, Weitao Chen and Qing Nie, A hybrid method for stiff reaction–diffusion equations, Discrete and Continious dynamical Systems Series B, 24 (2019) 6387—6417.

CONFLICT OF INTEREST

The authors have no conflicts of interest to declare. All co-authors have seen and agree with the contents of the manuscript and there is no financial interest to report. We certify that the submission is original work and is not under review at any other publication.